PCCP

Universal Crossed Beam Imaging Studies of Polyatomic Reaction Dynamics

Journal:	*Physical Chemistry Chemical Physics*
Manuscript ID	CP-PER-01-2020-000522.R1
Article Type:	Perspective
Date Submitted by the Author:	20-Mar-2020
Complete List of Authors:	Li, Hongwei; University of Missouri Columbia College of Arts and Science, Chemistry Suits, Arthur; University of Missouri Columbia College of Arts and Science, Chemistry

Universal Crossed Beam Imaging Studies of Polyatomic Reaction Dynamics

Hongwei Li and Arthur G. Suits*
Department of Chemistry, University of Missouri. Columbia, MO 65211, USA

Abstract:

The marriage between high level quantum calculations and experimental advances in laser technology, quantum state control, and detection techniques have opened the door to the study of molecular collision dynamics at a new level of detail. However, one current challenge lies in adapting these powerful strategies to address questions beyond the scope of the small ground state systems that have largely been the focus of reaction dynamics investigations to-date. For molecules with intermediate or large size (more than 6 atoms), lack of spectroscopic information and spectral congestion limit quantum state preparation, control and detection for experiment, and the large number of degrees of freedom of the system makes accurate quantum dynamics calculations prohibitively expensive. Nevertheless, studies of the chemical dynamics of such systems can reveal novel aspects of reactivity not anticipated based upon the behavior of smaller model systems. This Perspective will highlight applications of soft vacuum ultraviolet photoionization at 157 nm as a universal probe in combination with crossed beams and DC slice velocity map ion imaging to study bimolecular reaction dynamics of molecules of intermediate or large size, illuminated with support of high-level *ab initio* calculations. Here, we report on the chemical dynamics of atomic oxygen or chlorine reactions with organic compounds: propanol isomers, alkylamines ($N(CH_3)_3$ and $NH(CH_3)_2$), and isobutene ($(CH_3)_2CCH_2$) studied using this approach. The polyatomic radical products from the hydrogen abstraction process have been detected by 157 nm photoionization and their slice ion images embody translational energy and angular information that directly reflect the underlying collision dynamics. Various reaction mechanisms (such as direct abstraction and addition–elimination) along with the involvement of roaming dynamics and novel intersystem crossing pathways are presented. These demonstrate the power of this technique to reveal fundamentally new aspects of reaction dynamics that arise in larger reaction systems.

* *Author to whom correspondence should be addressed. E-mail: suitsa@missouri.edu*

1. Introduction

A predictive understanding of the chemical behavior of macroscopic systems – from high temperature combustion to interstellar clouds at 10K – requires knowledge of the elementary mechanisms and pathways to help bring order to the thousands of reactions that may be involved. The field of chemical reaction dynamics developed to address this challenge and it has achieved great success in using sophisticated experimental techniques to reveal underlying reaction mechanisms, chemical reaction rates, product branching and energy distributions, taking us far along the path to this full understanding.[1] The crossed molecular beam (CMB) technique holds a central place in these efforts, allowing the measurement of bimolecular reactions dynamics under single-collision conditions, measuring the nascent product translational energy and angular information during the reaction process.[2] The very first generation of CMB instrument was developed around 1954 by Bull and Moon[3] and followed shortly after by Taylor and Datz[4], when limited detection methods meant only reactions involving alkali species could be studied. The current success of the CMB method relies on the next generation universal instruments begun by Herschbach and Lee in 1969, which employed a rotatable electron bombardment ionization/mass spectrometer detector. This opened the door to the study of neutral–neutral reactions generally and brought scattering studies from the realm of physics firmly into place in the physical chemistry laboratory. This transformation presaged the current era in which, driven by advances in laser technology and detection strategies, the study of state-to-state molecular collision dynamics is now possible. These experimental advances, now coupled with parallel developments in high level quantum calculations, permit the study of chemical reaction dynamics in extraordinary detail.

Since the 1970s, these methods have been applied to achieve a deep understanding of chemical reaction dynamics for simple systems. The simplest prototypical reaction involves three atoms, generically written as A + BC → AB + C. Hydrogen exchange reactions, widely studied in crossed-beams using the high-resolution H/D-atom Rydberg tagging time-of-flight detection method, are the most important example of this class of reactions. Two different types of mechanisms are seen: the abstraction mechanism for the reactions of H + H_2,[5-9] F + H_2,[10-14] Cl + H_2,[15-18] and O(^{3}P) + H_2[19, 20] (and their isotopic variants), and the insertion mechanism for the reactions of O(^{1}D) + H_2,[21-23] N(^{2}D) + H_2,[24, 25] C(^{1}D) + H_2,[26-28] and S(^{1}D) + H_2[29-31] (and their isotopic variants). For these triatomic reactions, rigorous quantum mechanical methods can be applied on accurate *ab initio* potential energy surfaces (PESs) to calculate the state-to-state reactive differential cross section (DCS). The comparisons between the experimental and theoretical DCS allow study of the underlying reaction dynamics at an extraordinary level of detail. Interesting quantum phenomena such as reactive resonances have been observed in many triatomic reactions: F + H_2 /HD,[11, 32] Cl + HD,[18] and S($^1D_2$) +HD[31]. Very recently, the geometric phase effect has also been detected by Yuan *et al.* in the simplest hydrogen exchange reaction H + HD → H_2 + D for the first time.[33] At this point, it is clear that the reaction dynamics of these triatomic systems represent a triumph of joint experimental-theoretical investigation.

The problem becomes much more difficult when we extend our considerations to four-atom systems. The additional atom increases the number of degrees of freedom from three to six, and increases the number of quantum states in the system. In the triatomic reaction system, internal excitation is only considered in one vibrational and two rotational degrees of freedom of the reactant/product, whereas in four-atom reactions, the triatomic reactant/product in general has three vibrational and three rotational degrees of freedom. Now we must also determine how energy is distributed among different vibrational modes and what factors are responsible. Mode-specific behavior also becomes an important question in the reaction dynamics of four-atom systems,

resulting in more challenges for experimental measurements. The greater number quantum states will also tremendously increase the cost of high-level theoretical calculations and make it difficult or impossible to treat them fully quantum dynamically. To date, some four-atom reactions have been studied by both experiment and theory, although at a lower level of detail compared to the triatomic systems. These include OH + H_2[34-36] and its reverse reaction H + H_2O[37-39], CN + D_2,[40] $O(^3P)$ + H_2O,[41] OH + CO,[42, 43] F + H_2O,[44-46], and $N(^2D)$ + H_2O[47]. Of these only OH + H_2[36] and F + H_2O[45] have been treated with full-dimensional quantum calculations. Thus, even four-atom reaction dynamics are still just on the way to a full understanding.

Beyond four-atom reaction will be polyatomic reactions that contain a reactant with more than three atoms. Studying polyatomic reaction dynamics is obviously more challenging than three- and four-atom reactions, because of the additional degrees of freedom, more reaction pathways, etc. One widely-studied class of polyatomic reactions that involves small molecules (containing ≤ 6 atoms) is that of methane (and its isotopologues): X + CH_4, where X is H[48], F[49-51], Cl[52-54], $O(^3P)$[55, 56], and OH[57, 58] (involving direct abstraction), or X is $O(^1D)$[59-61], $N(^2D)$[62], $C(^1D)$[63], and $S(^1D)$[64] (involving indirect insertion). The methane-family reactions were systematically studied by Liu and coworkers by imaging reactive scattering of the methyl radical product with resonance-enhanced multiphoton ionization (REMPI) in a CMB experiment.[49-58] The mode- and bond-selected reactivity in the methane reactions were investigated and a range of interesting phenomena were observed in the correlated state distributions, including reactive resonances, reactive "rainbows", and stereochemistry.[65]

Most practical chemical problems such as combustion or atmospheric chemistry involve larger molecules, and such systems can exhibit profound changes in dynamical behavior relative to small molecules, making extrapolation dangerous and intuition unreliable. However, the increase in the size of the system dramatically increases the difficulty to study them, both from experimental and theoretical perspectives. For larger molecules, i.e. hydrocarbons with more than two carbon atoms, lack of spectroscopic information and spectral congestion limit their quantum state preparation, control and detection. It is almost impossible to measure the state-to-state reactive DCSs for bimolecular reaction of molecules that are of intermediate or large size. The crossed molecular beam instruments with universal rotatable mass spectrometric detection has become a powerful general tool for the study of the reaction dynamics as first developed by Lee and coworkers.[66] Later, Kaiser and coworkers applied this technique to look into gas phase synthesis of large molecules that are important in the astrochemistry[67-69], for example in studies of the reactions of phenyl (C_6H_5)[70-72], ethynyl (CCH)[73, 74], cyano (CN)[75, 76], silicon nitride (SiN)[77, 78], boron monoxide (BO)[79, 80] radicals with the unsaturated hydrocarbons. Many combustion related elementary reactions, i.e. atomic oxygen reaction with unsaturated hydrocarbons, were also studied via CMB instruments first by Lee and coworkers[66, 81-83], and recently systematically investigated by Casavecchia and coworkers[84-91].

In recent years velocity map imaging has emerged as a powerful alternative approach for the study of CMB reactions as mentioned above for the methane reactions. This has some advantages complementary to those of the traditional mass spectrometric instruments, most importantly state-specific or universal detection and the lack of kinematic constraints. This Perspective will highlight our applications of soft vacuum ultraviolet (VUV) photoionization as a universal probe at 157 nm in combination with crossed beams and DC slice velocity map ion imaging. Fundamentally new aspects of reaction dynamics that arise in larger reaction systems have been investigated using this approach and selected examples will be presented in this Perspective. The growth in computational power and development of new algorithms over the past

decade or two has also been such that now high-level electronic structure and dynamical calculations provide essential insight into the underlying reaction mechanisms. The calculated potential energy surfaces reveal possible reaction intermediates, transition states and corresponding products along the reaction pathways that are essential to interpret the experimental results. This synergy between experiment and computation is a crucial ingredient in advancing CMB methods for larger systems that emerged in the mid-1990s and is now central to almost all such studies.[92, 93]

2. Crossed-beam DC slice imaging approach

The ion imaging technique was invented by Chandler and Houston in 1987 to measure state-resolved product translational energy release and angular distributions from photodissociation events.[94] The neutral photofragments of interest were ionized by a probe laser and the recoiling ion sphere was accelerated in a Wiley-McLaren[95] time-of-flight mass spectrometer onto a 2D microchannel (MCP) detector. The detector was coupled to a phosphor screen to visualize each ion spot, which was viewed and recorded by a camera. A key advance for ion imaging, the velocity map imaging (VMI) technique, was developed by Eppink and Parker in 1997.[96] They replaced the grids of the Wiley-McLaren mass spectrometer with ion lenses, permitting focusing of ions to a point based only on their velocity perpendicular to the flight direction, regardless of their birthplace in the interaction regions. This simple innovation, readily implemented, yielded an order of magnitude improvement in velocity resolution, now unmatched by other techniques. Since then, VMI has become very widely used to study unimolecular dissociation, scattering and photoelectron spectroscopy as well. In 1999, Ahmed and coworkers applied VMI technique in a crossed beam experiment for the first time, measuring the product scattering information for the $O(^1D) + D_2 \rightarrow OD + D$ reaction with D atom ionized by 1+1′ REMPI.[97] Around the same time, the Davis group at Cornell introduced the use of the F_2 excimer laser for single photon VUV ionization at 157 nm as a robust and convenient ionization source. They coupled it with a dual rotatable source crossed beam apparatus with quadrupole mass spectrometer detection.[98] Since metal hydrides and metal-binding carbohydrates can be ionized readily by a single photon at 157 nm, they were able to systematically study reactions between transition metals (such as Y, Zr, Mo, V, and Nb) and hydrocarbons (such as CH_4, C_2H_4, C_3H_6, *c*-C_3H_6, C_4H_8, CH_3CCH, CH_3CCCH_3, *c*-C_6H_{12}, H_2CO, CH_3CHO, $(CH_3)_2CO$).[99-110] In addition to metal complexes, the non-terminal alkyl (C3 and larger), hydroxyalkyl, and aminoalkyl radicals have ionization energy less than 7.9 eV and can be photoionized by single photon of 157 nm. Those radicals or molecules that have ionization energy slightly higher than 7.9 eV can also be ionized by 157 nm under two-photon processes with a focused laser beam. Based on these advantages, our group first coupled 157 nm photoionization with velocity map imaging in 2000.[111] The first such study was imaging of H abstraction dynamics for Cl + ROH reactions,[111] followed by systematic investigation of reaction dynamics of large hydrocarbons with a range of radicals.[112-125] Another innovation, DC sliced[126] or time-sliced imaging[127, 128], followed shortly after the advent of VMI. In this approach, rather than projecting the entire ion cloud onto the 2-D detector and mathematically reconstructing the 3-D distribution, one stretches the ion cloud along the flight direction with an initial weak acceleration field, allowing for gating the central slice of the distribution for detection.

The crossed molecular beam technique provides the ability to study chemical reactions under single collision conditions, i.e. without wall effects or third body collisions, so that the nascent product translational energy and angular distribution information are measurable to

unravel the underlying dynamics. Our experimental setup is illustrated in Figure 1 and described in detail previously.[121, 122, 129, 130] Briefly, the apparatus consists of one reaction chamber and two source chambers fixed perpendicular to each other. Both molecular beams are pulsed and supersonically expanded into source chambers using piezoelectric stack valves[131] then skimmed into the reaction chamber. Differential pumping maintains the two source chambers to be ~10^{-8} torr base and ~10^{-5} torr operational pressures, and the reaction chamber as ~10^{-7} torr or below to satisfy single-collision conditions. Radical precursors and hydrocarbons are diluted in different carrier gases (H_2/He/Ne/Ar) in order to vary the collision energy of the reaction. Radical molecular beams can be generated by photolytic sources, discharge sources, and flash pyrolysis sources depending on the radical desired. For example, as shown in Figure 1, the electronic ground state $O(^3P)$ beam was generated from the photolysis of SO_2 by the 193 nm output of an ArF excimer laser, which was loosely focused via a cylindrical lens along the length of a capillary tube attached to the pulsed valve nozzle. Both molecular beams were collimated by a 1-mm-diameter skimmer before entering the reaction chamber, and crossed with each other at an angle of 90° in the interaction region. Following reaction, the scattered products were ionized with VUV 157 nm radiation (7.9 eV) from a commercially available nanosecond pulsed F_2 excimer laser. Ions were initially accelerated by a five-electrode DC slice ion optics assembly, and velocity-focused onto a position-sensitive detector after passing through a 75 cm field-free flight tube. The position-sensitive detector consists of a phosphor screen and a dual MCPs with back MCP gated to the center slice of the scattered product ions at a specific *m/z* channel. The slice ion images were recorded using a CCD camera, analyzed with a high-resolution real-time ion counting method by our own megapixel acquisition program NuACQ[132]. Background subtraction and density-to-flux corrections were performed prior to transforming the scattering distribution into the center-of-mass flux distributions. Background images were recorded sequentially rather than shot-to-shot with stable conditions, and density-to-flux correction was performed by scaling the pixel intensity by the lab velocity at each point on the image.

3. Applications to polyatomic reaction dynamics

Here we examine the chemical dynamics of atomic oxygen or chlorine reactions with selected organic compounds chosen to highlight particular aspects of polyatomic dynamics that diverge in important ways from those of smaller systems. These reaction targets are propanol isomers[125], alkylamines ($N(CH_3)_3$ and $NH(CH_3)_2$)[124], and isobutene ($(CH_3)_2CCH_2$)[120], studied using our CMB apparatus described in the previous section. Three different reaction examples with three different reaction mechanisms will be presented here to elucidate the power of this combination of a sensitive universal VUV probe with crossed molecular beams and DC slice velocity map imaging detection.

3.1 $O(^3P)$ + propanol isomers

Biofuels have been of increasing interest as alternatives to petroleum-based transportation fuels because they are renewable and carbon-neutral, thereby offering a long-term fuel-source with less impact on the air pollution and climate change. For effective development of such fuels, it is necessary to model practical combustion environments from fundamental principles. This requires knowledge of the nature and identity of the elementary reaction mechanisms, the size of any activation barriers, the identity of reaction products and the thermochemistry and energy disposal in the relevant species. CMB experiments provide the opportunity to study these detailed underlying dynamics for elementary reactive processes. Propanol isomers have been proposed as

one potential biofuel[133], and their reaction dynamics with ground state atomic oxygen have been studied by CMB with our VUV universal probe and DC slice velocity map imaging detection[125] for the first time.

The hydroxypropyl radical products from the reaction of $O(^3P)$ with 1-propanol and 2-propanol at collision energies of 8 and 10 kcal mol^{-1} have been detected with 157 nm photoionization and their scattering images are shown in Figure 2, with the derived total translational energy release $P(E_T)$ and angular $T(\theta)$ distributions on the right panels. Based on *ab initio* ionization calculations at the CBS-QB3 level of theory, all of the possible hydroxypropyl radical products may be detected at 157 nm, and the reaction enthalpies are as follows:

$$O(^3P) + CH_3CH_2CH_2OH \rightarrow CH_3CH_2CHOH + OH\ (X^2\Pi)$$
$$\Delta_rH\ (0K) = -7.8\ \text{kcal mol}^{-1} \quad (1)$$
$$O(^3P) + CH_3CH_2CH_2OH \rightarrow CH_3CHCH_2OH + OH\ (X^2\Pi)$$
$$\Delta_rH\ (0K) = -3.4\ \text{kcal mol}^{-1} \quad (2)$$
$$O(^3P) + (CH_3)_2CHOH \rightarrow (CH_3)_2COH + OH\ (X^2\Pi)$$
$$\Delta_rH\ (0K) = -9.9\ \text{kcal mol}^{-1} \quad (3)$$

The first 40° of the forward component relative to the propanol beam direction was excluded in the analysis for both reactions because of the intense photochemical signal created by the probe laser only. Nevertheless, the angular distributions, $T(\theta)$, shown in the inset of Figure 2 clearly indicate a backward-scattered distribution that implies direct rebound dynamics. This rebound dynamics involves small impact parameter collisions, leading to direct reaction *via* a collinear transition state geometry, O-H-C, that is suggested by the well-established line-of-centers triatomic model[134, 135] and is also identified in the stationary point calculations[125, 136, 137]. Assuming a pseudo-triatomic picture in which the hydroxypropyl radical is a structureless quasi-atom, a simple kinematic model suggested by Evans *et al.*[138] can be employed for the colinear triatomic collision system to predict the average translational energy release: $\langle E_T \rangle = E_c\cos^2\beta + E_R\sin^2\beta$. Here β is the skew angle defined for A + BC system by $\cos^2\beta = (m_A m_C)/(m_{AB} m_{BC})$, E_c is the collision energy, and E_R is the reaction energy. For the $O(^3P)$ reaction with both propanol isomers, the skew angle is acute, as typically seen in heavy-light-heavy hydrogen transfer reactions, so the first term strongly dominates, predicting that the average translational energy release is very close to the collision energy. However, the experimentally measured translational energy release only accounts for 40-50% of the collision energy. The reduced translational energy release relative to the triatomic model is not surprising, and suggests that internal energy in the hydroxypropyl radical is important. A modification of the triatomic model referred to as a "vertical" H abstraction mechanism[112, 139] was applied to estimate the internal excitation of the hydroxypropyl radical. This Franck-Condon picture considers that the C-H bond breaks so rapidly that the hydroxypropyl radical cannot relax to its minimum energy geometry resulting in a certain amount of energy "locked" in the C_3H_6OH moiety, in this case about 10-30% of the total available energy. OH vibrational excitation could take about 10-30% of the total available energy as suggested by the relevant reactions of $O(^3P)$ + saturated alkanes by Andresen and Luntz[134, 140]. These considerations then suggest that the most of the available energy (about 30-50%) is partitioned into the rotational excitation of the radical products, especially the OH $X^2\Pi$ radical with its large rotational constant, 18.91 cm^{-1}.[141] This rotational excitation can be induced by the long-range dipole–dipole interaction between the OH and hydroxypropyl radicals. Both radical products have large dipole moments, 1.6676(9) D for OH[142], and 1.282 D, 2.182 D, and 1.653 D for CH_3CH_2CHOH, CH_3CHCH_2OH,

and $(CH_3)_2COH$ radical, respectively[125]. The role of the long-range dipole–dipole interaction between the product pair, obviously not available to a triatomic reaction system, is also supported by the presence of the post-transition state (post-TS) exit channel complex (bound by 3-5 kcal mol^{-1}) in all H abstraction pathways.[125, 137] Similar post-TS dipole–dipole interaction behavior was observed in the Cl atom reaction with oxygen-containing organic compounds by Orr-Ewing and coworkers.[143] Very recently, Troya investigated the O(^{3}P) + 2-propanol hydrogen abstraction reaction by *ab initio* and quasiclassical trajectory (QCT) calculations using a specific-reaction-parameters PM6 semiemipirical Hamiltonian with all conformers and abstraction sites taken into account.[137] Very good agreement on the product translational energy release and angular distributions of this reaction was achieved between the QCT calculations and our experimental results (shown in Figure 2), although QCT suggested that most of the available energy is deposited into the vibrational excitation of the hydroxypropyl radical. This will need further measurements on the OH product state distributions in order to confirm the internal energy disposals.

3.2 O(^{3}P) + alkylamines reaction

Reactions of nitrogen containing organics are important for their prebiotic potential in astrochemistry[144] and for their chemical conversion to nitrogen oxides (NO_x) in combustion processes[145]. The bimolecular reaction dynamics of the elementary reactions of alkylamines (dimethylamine and trimethylamine, herein DMA and TMA) with atomic oxygen O(^{3}P) have been studied for the first time by Li *et al.* using CMB with 157 nm VUV probe and velocity map imaging detection and those results illustrate another novel finding arising in part from the dipole-dipole interaction between the products.[124]

In both O(^{3}P) reactions with DMA and TMA, the aminoalkyl radical products (CH_3NHCH_2 and $(CH_3)_2NCH_2$) generated by H abstraction from the methyl site were probed via 157 nm single photon ionization. The abstraction site in DMA was confirmed by both *ab initio* ionization energy calculations and the use of a partially deuterated isotopologue, $(CD_3)_2NH$. The corresponding product scattering images after background subtraction and density-to-flux correction are shown in Figure 3, with a nominal Newton diagram superimposed. The scattered radical products are examined in three distinct center-of-mass (c.o.m.) angular ranges defined with respect to the alkylamine beam direction: forward (0-60°), sideways (60-120°), and backward (120-180°). Despite the fact that the forward component is obscured by the strong photochemical background, the sideways and backward components still provide enough information to reveal the underlying dynamics. Interestingly, in contrast to the observations of the direct H abstraction dynamics that we saw in the O(^{3}P) + propanol isomers reaction, the O(^{3}P) reactions with DMA/TMA clearly indicate an indirect reaction mechanism. As shown in Figure 3, the c.o.m. translational energy release distributions $P(E_T)$ peak at very low energy, ~10% of the collision energy, with nearly identical $P(E_T)$ distributions for both sideways and backward components. The c.o.m. angular distributions $T(\theta)$ are also flat, consistent with the isotropic images observed. Both low translational energy release and isotropic angular distributions of the scattered products indicate the important of the long-lived complex formation prior to OH elimination mechanism in these reactions. Formation of a long-lived complex in a bimolecular reaction results in less product translational energy release as the internal energy can randomize over the large number of vibrational degrees of freedom in the long-lived complex. Furthermore, if the lifetime of the complex is longer than its rotational period, the system loses reference to the initial approach direction, giving rise to a symmetric forward-backward scattering distribution and identical

translational energy distributions. For complicated polyatomic systems where the scattering is not planar, this symmetric scattering often becomes fully isotropic as we observe in this experiment.

A careful search along the PESs of the O(^{3}P) + DMA/TMA reaction was performed to identify the pathway for OH elimination from the long-lived complex that we have observed experimentally. Both reactions have similar PESs and key stationary points for the O(^{3}P) + DMA reaction are shown here in Figure 4. On the triplet PES, barrierless direct H abstraction (purple dashed line) and a long-range "roaming-type" transition state (TS-Roam, red line) pathways have been found. The latter has an exit channel well of only 4 kcal mol^{-1} deep with respect to the product asymptote. Such a well could not account for the long lifetime of the complex that has been observed in the experiment. The direct H abstraction process on the triplet surface was simulated with direct dynamics using a Born-Oppenheimer molecular dynamics model. The simulation shows that the direct H abstraction process is complete within 1 ps giving rebound dynamics, but more interestingly, it also indicates extensive reorientation and interaction between the newly formed OH and aminoalkyl radical products. This is likely due to the long-range dipole–dipole interaction similar to the post-TS dipole–dipole interaction behavior that we have inferred in the O(^{3}P) + propanol reaction study. This interaction also suggests the possibility of intersystem crossing (ISC) to the singlet surface in the exit channel that could bring the system to the strongly bound singlet hydroxyalkylamine well prior to forming the detected products. ISC could not occur in the entrance channel because the high barrier on the singlet surface precludes formation of the detected products. High-level multireference *ab initio* calculations were carried out for the exit channel region as indicated by the blue shaded box in Figure 4, showing that the first two singlet and the first two triplet PESs are degenerate, with singlet–triplet splitting from 0.3 to 2.3 kcal mol^{-1} in this region. Two pairs of singlet–triplet states, S_0-T_2 and S_1-T_1, were also found to have strong spin–orbit couplings. The orbitals participating in the wavefunctions of S_0, S_1, T_1, and T_2 are shown in the inset in Figure 4, including two orthogonal *p* orbitals in the OH radical (MO1 and MO2). Switching from the triplet to singlet state only requires one electron to change between MO1 and MO2, which allows the *p* electron to change its orbital angular momentum and spin simultaneously, satisfying the El-Sayed rule[146, 147] for ultrafast ISC. Although ISC has been long known in bimolecular reactions of atomic oxygen with alkenes[66, 81-83], it occurs there by formation of a long-lived diradical complex (normally bound by >20 kcal mol^{-1}) whose lifetime permits ISC[84-91]. In contrast, here it is two radicals (OH and CH_3NHCH_2) interacting in the exit channel, where there are degenerate triplet and singlet PESs, relatively strong spin–orbit coupling, and satisfaction of the El-Sayed rule, that permits very efficient ISC to access to the very deep well on the singlet surface rather than being caused by it.

3.3 Cl($^2P_{3/2}$) + isobutene reaction

Broadly speaking, radical–molecule reactions can undergo two different reaction mechanisms, direct and indirect processes. The direct mechanism can be direct H abstraction, *e.g.*, the O(^{3}P) + propanol reactions as discussed in Section 3.1, and the indirect mechanism can be addition–elimination, *e.g.*, the O(^{3}P) + alkylamines reaction as discussed in Section 3.2. The reactions of Cl atom with alkenes interestingly have both the direct H abstraction pathway (Cl abstracting H of the methyl group), and the indirect addition–elimination pathway (Cl initially adding to the double bond before HCl elimination).[117, 119, 120, 148-150] However, both the direct H abstraction and the indirect addition–elimination pathways go to the same exit channel complex with identical final products, making it difficult to distinguish between these two reaction pathways based on the internal energy in the products. A dynamics study of Cl($^2P_{3/2}$) atom reaction

with four butene isomers was reported by Joalland *et al.* using DC slice imaging in a CMB experiment with 157 nm ionization detection of the alkenyl radical product (HCl is the coproduct).[119] Detailed analysis of the measured angular and translational energy distributions provided important evidence to identify both direct and indirect reaction processes. Direct H abstraction contributions were apparent in the forward-backward asymmetry in the angular distribution, and the translational energy release of the forward component seemed more likely to preserve the collision energy than that of the sideways and backward components. This distinction is greatest for 1-butene, intermediate for the two 2-butenes, and least for isobutene. The lower translational energy release in the case of the isobutene reaction indicates that more product internal excitation resulted from energy randomization in the long-lived adduct, suggesting a greater contribution from the indirect addition–elimination process. However, a preliminary survey on the PES failed to identify a conventional TS for HCl elimination from the adduct. One possible explanation for this is that the decomposition occurs via a Cl atom roaming mechanism. Roaming reactions, first reported in formaldehyde photodissociation, involve frustrated dissociation to radical products followed by reorientation and intramolecular reaction leading to unexpected products or a distinct product state distribution.[151, 152]

Further investigation of Cl reaction dynamics with isobutene were performed at three different collision energies, 14, 8, and 4 kcal mol^{-1} to have a deeper look into this question.[120] The corresponding product translational energy release and angular distributions under these collision energies successfully revealed the two different mechanisms. At E_c = 14 kcal mol^{-1} (shown in the left panel of Figure 5), the translational energy distribution in the FW direction peaks at significantly higher energy than in the SW and BW directions, and the angular distribution shows a FW scattering pattern. This indicates direct H abstraction dynamics with more stripping components that involve little energy and momentum transfer. For the intermediate collision energy E_c = 8 kcal mol^{-1} (middle panel of Figure 5), the angular distribution becomes slightly flattened, indicating an evolution to a more isotropic scattering with decreasing collision energy. At the meantime, the translational energy distribution in the FW direction peaks to lower energy region and becomes more similar to the SW/BW distributions. At E_c = 4 kcal mol^{-1} shown in the right panel of Figure 5, the angular distribution is fully isotropic and the translational energy release peaks near 0 kcal mol^{-1}, despite that reliable data could not be obtain for the FW component because of the interference from the photochemical background. Long-lived complex formation followed by HCl elimination mechanism now starts to play an important role as the collision energy is lowered. Although it was not possible to quantify the relative contributions of direct versus indirect reactions from these experiments, varying the collision energy has clearly shown a role for both as the collision energy is increased.

The related Cl + propene reaction has been reported from several studies by Orr-Ewing and coworkers.[148-150] Most recent QCT studies on a global PES constructed by an empirical valence bond fit to the high level *ab initio* stationary points allowed them to obtain the branching between the direct and the indirect processes. The trajectory calculations indicated that the contribution of the direct abstraction reaction dominates at high collision energy and decreases with decreasing collision energy[150], consistent with the trend reported for isobutene reaction by Joalland *et al.*. Both Cl + propene and isobutene reactions have similar PESs, with one barrierless direct H abstraction pathway and one indirect addition–elimination pathway following adduct stabilization at ~20 kcal mol^{-1}. Both pathways connect to the same complex in the exit channel that can decay to HCl and alkenyl radical products, but a key question is the reaction path leading from the strongly bound adduct to HCl elimination. The CBS-QB3 level of theory applied to the

isobutene reaction could not find a conventional tight TS for the addition–elimination pathway. However, a peculiar/quasi-bound TS was located just 1.6 kcal mol^{-1} below the reactant asymptote. This quasi-bound TS as shown in the inset of the right panel in Figure 5 has C-Cl distances of 3.5 and 3.9 Å, and Cl-H distance of 2.4 Å. The imaginary frequency of this TS is only 317 cm^{-1} (a flat surface indicated here) with vibrational motion of Cl-atom wandering around the isobutene moiety, and another two very low bound frequencies were calculated (45 and 78 cm^{-1}) corresponding to motions of the Cl-atom relative to the isobutene fragment. The remaining frequencies were very similar to those of isobutene except for one C-H stretching mode that is reduced to 2,706 cm^{-1} because this bond is slightly elongated and prepared to be H abstracted by the Cl atom. All these suggest a roaming radical mechanism, in which the Cl atom leaves the CC double bond, is about to be eliminated (returning back to reactants), but wanders in the direction of the allylic site and abstracts a H atom from the methyl group to form HCl. This is comparable to the well-known roaming system in the unimolecular dissociation of H_2CO or the related H + HCO bimolecular reaction if starting from this reactant asymptote, where a roaming-type TS has low frequencies of 140*i*, 20 and 80 cm^{-1}.[153]

4. Conclusions and outlook

We have highlighted recent applications of our crossed molecular beam imaging approach using a single-photon VUV ionization probe at 157 nm to study polyatomic reaction dynamics. The universal probe allows us to study many polyatomic reactions where spectroscopic probes such as REMPI or LIF are not possible. Three different reaction examples were shown, each highlighting novel dynamics arising in reactions of larger polyatomic systems. In the $O(^3P)$ + propanol isomers reaction, direct rebound dynamics were observed with high internal excitation deposited in the reaction products. In the $O(^3P)$ + alkylamines reaction, indirect long-lived complex formation prior to OH elimination mechanism was revealed in the experiment. The long-lived complex arises from the deep hydroxylamine well on the singlet surface, which is accessed by intersystem crossing occurring in the exit channel of the reaction. Such exit channel dynamics would not be readily anticipated based on extrapolation from smaller systems. The Cl + isobutene reaction has both the direct H abstraction and the indirect addition–elimination pathways. By tuning the collision energy, two different reaction mechanisms were found in the experiment. *Ab initio* calculations then showed that roaming dynamics are central to the addition–elimination pathway. These three examples with different reaction dynamics demonstrate the power of this technique to reveal fundamentally new aspects of reaction dynamics that arise in larger systems.

In the future, OH radical reactions with large polyatomic alkanes and alkenes can be studied which are important in the atmosphere and in combustion and astrochemistry. The alkyl radicals from the reactions of OH with alkanes can be readily detected by 157 nm VUV probe. On the other hand, alternative VUV ionization probes with higher photon energies could be implemented so that additional molecular and radical products can be detected. The Davis group at Cornell recently demonstrated a powerful method to generate high intensity VUV radiation (0.1 mJ pulses at 125 nm, 6×10^{13} photons/pulse) by resonance enhanced four-wave mixing of two or three unfocussed dye lasers in heated mercury (Hg) vapor.[154] VUV radiation from 130.2 nm to 120 nm was achieved by tuning dye lasers to pump atomic Hg to different electronic levels. Combining this VUV generation as a universal probe with crossed molecular beams and velocity map imaging detection will be very powerful to extend these studies to a wider range of chemical reaction systems.

One shortcoming in the present approach is the photochemical background interference that occurs when one of the reactants may be dissociated by the probe laser to give the same product as the reaction of interest. For instance, in our case when 157 nm probe ionizes reaction products, it also photodissociates the target hydrocarbons in the molecular beam and ionizes their photofragments with another photon. The photofragment ions overlap with the part of the reactive scattered product ions on the image if both ions have same mass-to-charge ratio, making it very challenging to obtain reliable information in the overlapping region. One possible solution for this would be to significantly slow down the hydrocarbon beam, for example, using cryogenic cooling of the valve with heavy carrier gas. Colliding with the other fast radical beam, the center-of-mass direction will further separate from the hydrocarbon beam direction, such that the background photofragment signal would not overlap with scattering product ions. Additionally, changing the intersection angle to more than 90º will also be helpful to separate center-of-mass further away from the target hydrocarbon beam.

Finally, we note an area of keen current interest is the study of chemical reaction dynamics at low collision energies where interesting quantum phenomena such as resonances and tunneling dominate. Recently, we reported an intrabeam/near-copropagating molecular beam apparatus that permits tuning the collision energy from above room temperature to 1 kelvin or below.[155, 156] This and related approaches have been used to examine inelastic scattering[157-159] and Penning ionization[160-165] for a range of systems, but this can be adapted for reactive scattering studies at low collision energy as well. As these approaches are implemented we can anticipate more surprises and more insight into the dynamical behavior of a wide range of reactive systems.

Conflicts of Interest

There are no conflicts of interest to declare.

Acknowledgements

This work was supported by the Director, Office of Science, Office of Basic Energy Science, Division of Chemical Science, Geoscience and Bioscience of the U.S. Department of Energy under Contract No. DE-SC0017130.

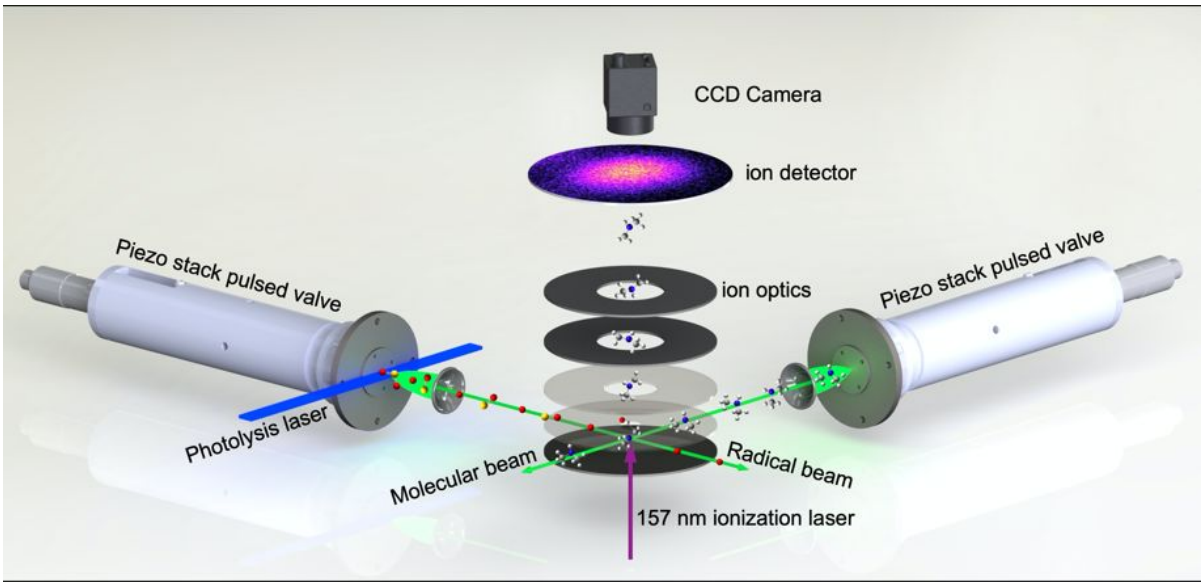

Figure 1. Schematic view of the crossed-beam apparatus combined with a universal DC slice imaging detection.

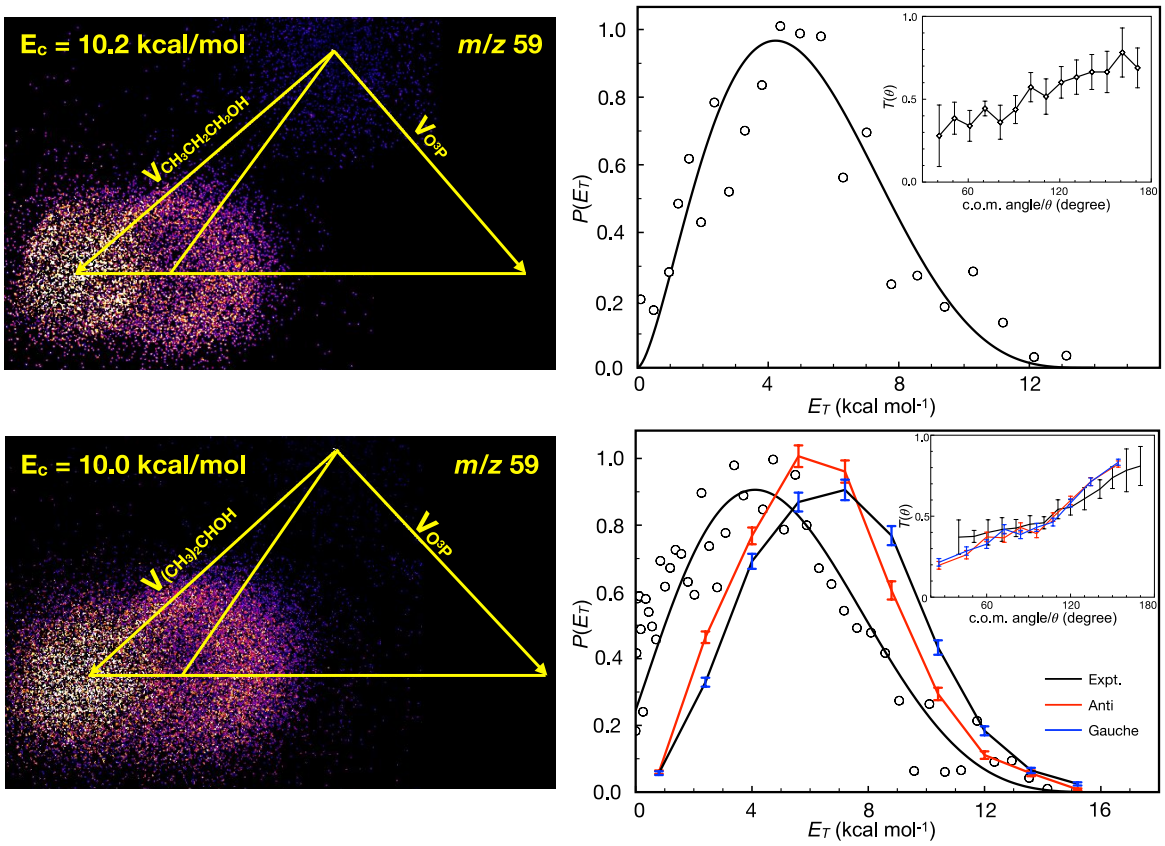

Figure 2. DC sliced scattering images for the reaction of O(^{3}P) with 1-propanol (top) and 2-propanol (bottom) at a collision energy of ~10 kcal mol^{-1}. Their corresponding translational energy release P(E_T) distributions are shown on the right with inset of the center-of-mass angular T(θ). The T(θ) distribution are shown averaged every 10° with error bars (±σ) estimated by mean absolute deviation of the raw data in the corresponding angular range. Adapted from ref. 126 with permission from the PCCP Owner Societies. For the O(^{3}P) + 2-propanol reaction, the experimental (black color) translational energy release and angular distributions are compared to QCT results from ref. 138 considering both anti (red color) and gauche (blue color) conformers of 2-propanol, shown in the bottom and right panel. Adapted with permission from ref. 138. Copyright 2019 American Chemical Society.

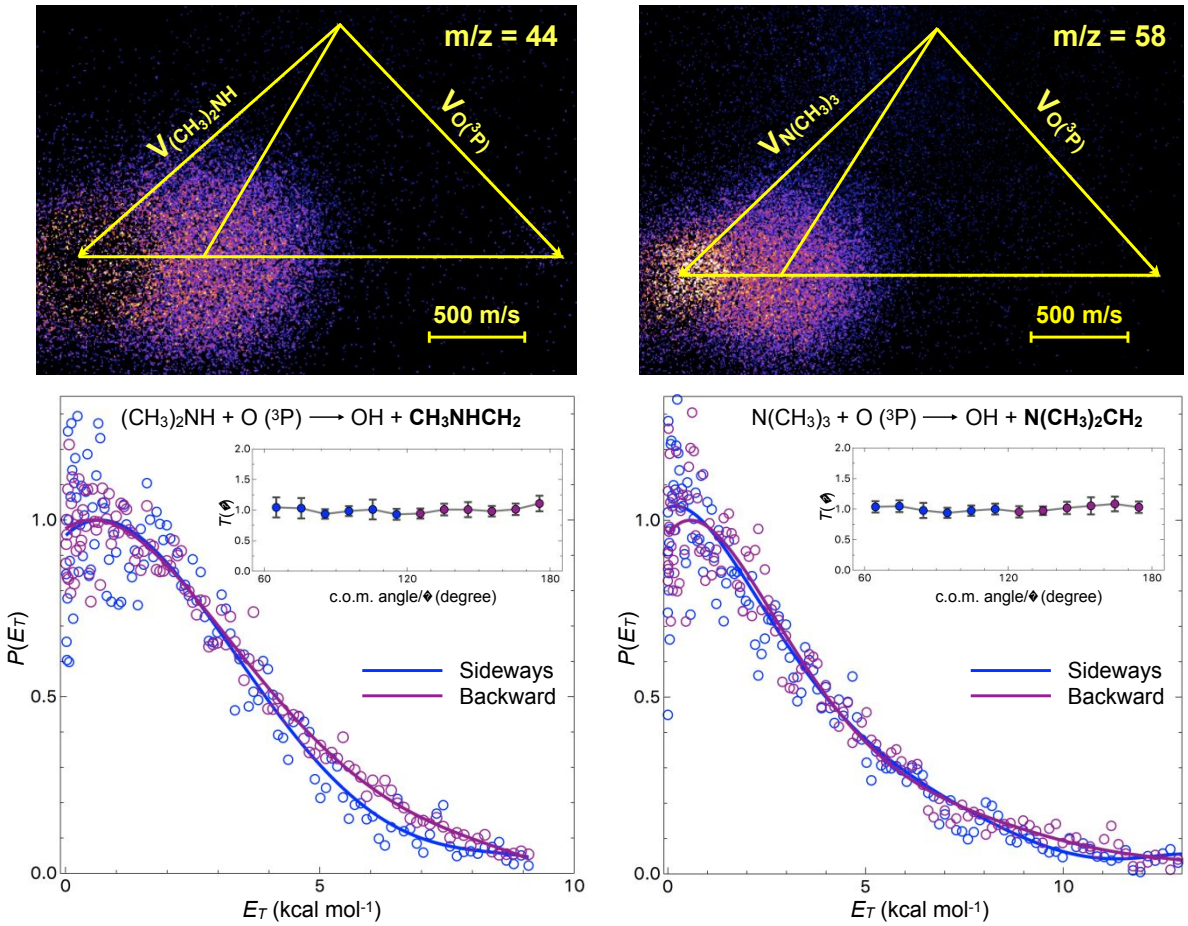

Figure 3. Velocity-flux contour map analysis of aminoalkyl products from reactions of $O(^3P)$ with $(CH_3)_2NH$ (left panel) and $N(CH_3)_3$ (right panel) at collision energies of 8.0 and 7.8 kcal mol^{-1}, respectively.[124] DC slice images of aminoalkyl products with Newton diagrams superimposed are shown on the top and their corresponding translational energy $P(E_T)$ distributions are shown on the bottom with the inset of the center-of-mass angular $T(\theta)$ distributions. The $T(\theta)$ distribution are shown averaged every 10° with error bars ($\pm\sigma$) estimated by mean absolute deviation of the raw data in the corresponding angle range. The sideways (60-120°) component is in blue and the backward (120-180°) component is in purple.

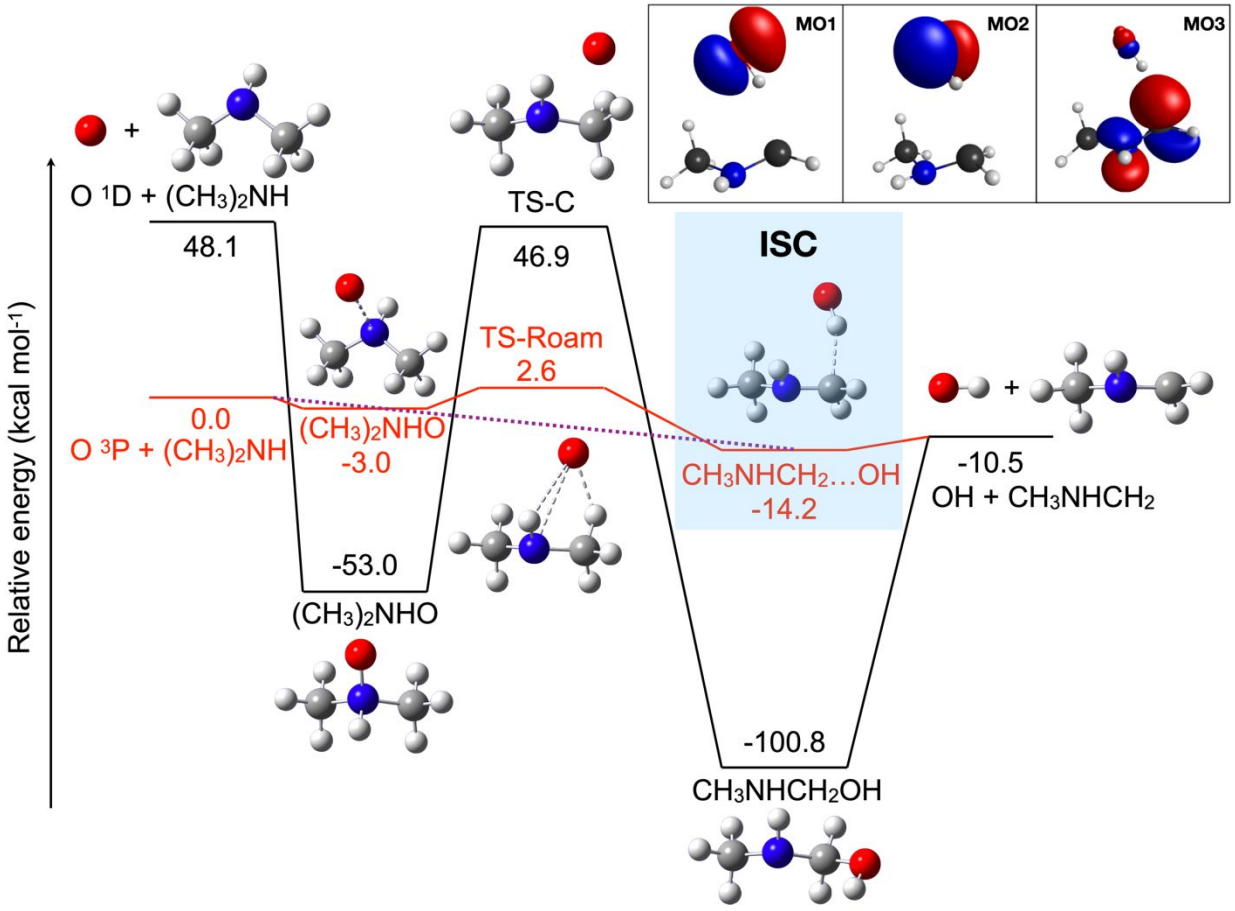

Figure 4. Key points on the triplet (red/purple line) and singlet (black line) PESs of the O(^{3}P) + DMA reaction at the CBS-QB3 level of theory with relative energies shown in kcal mol^{-1}.[124] Inset upper right shows orbitals participating in the wavefunctions of S_0, S_1, T_1, and T_2, taken from the CASSCF(4,4) calculation at the CH_3NHCH_2…OH geometry where intersystem crossing (ISC) occurs as indicated by the blue shaded box.

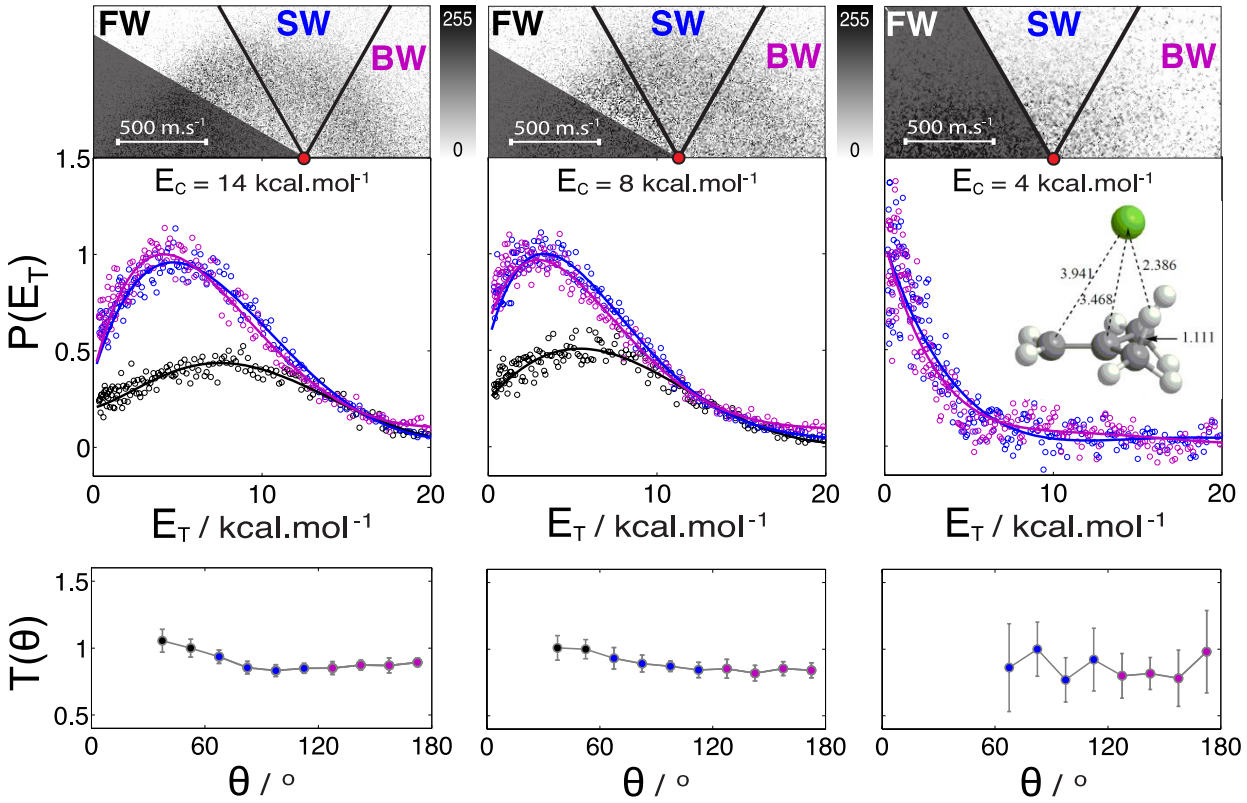

Figure 5. Velocity-flux contour map analysis of the C_4H_7 radical for different collision energies. Translational energy distributions $P(E_T)$ and angular distributions $T(\theta)$ are plotted for forward (FW, 30-60°, black), sideways (SW, 60-120°, blue) and backward (BW, 120-180°, purple) scattered products. The $P(E_T)$ are fitted by least squares polynomial regressions. The $T(\theta)$ are shown averaged every 15° with error bars estimated by mean absolute deviation of the raw data in the corresponding angle range. The corresponding velocity-flux contour maps are shown with the photochemical background masked. The red spots correspond to the center-of-mass at the three different collision energies (E_c = 14, 8, and 4 kcal mol^{-1}). Inset in the right panel shows the roaming-type transition state that connects the entrance addition complexes (that have around 20 kcal mol^{-1} adduct stabilization energy) and the exit van der Waals complex (that eliminates HCl to form the detected C_4H_7 radical product). The numbers in the inset list the lengths of indicated bonds (Å). Reprinted from reference 120.

References

1. R. D. Levine, *Molecular Reaction Dynamics*, Cambridge University Press, Cambridge, 2005.
2. Y. T. Lee, *Science*, 1987, **236**, 793-798.
3. T. H. Bull and P. B. Moon, *Discuss. Faraday Soc.*, 1954, **17**, 54-57.
4. E. H. Taylor and S. Datz, *J. Chem. Phys.*, 1955, **23**, 1711-1718.
5. D. Neuhauser, R. S. Judson, D. J. Kouri, D. E. Adelman, N. E. Shafer, D. A. V. Kliner and R. N. Zare, *Science*, 1992, **257**, 519-522.
6. T. N. Kitsopoulos, M. A. Buntine, D. P. Baldwin, R. N. Zare and D. W. Chandler, *Science*, 1993, **260**, 1605-1610.
7. L. Schnieder, K. Seekamp-Rahn, J. Borkowski, E. Wrede, K. H. Welge, F. J. Aoiz, L. Bañiares, M. J. Mello, V. J. Herrero, V. S. Rábanos and R. E. Wyatt, *Science*, 1995, **269**, 207-210.
8. S. A. Harich, D. Dai, C. C. Wang, X. Yang, S. D. Chao and R. T. Skodje, *Nature*, 2002, **419**, 281-284.
9. D. Yuan, S. Yu, W. Chen, J. Sang, C. Luo, T. Wang, X. Xu, P. Casavecchia, X. Wang, Z. Sun, D. H. Zhang and X. Yang, *Nat. Chem.*, 2018, **10**, 653-658.
10. D. M. Neumark, A. M. Wodtke, G. N. Robinson, C. C. Hayden and Y. T. Lee, *J. Chem. Phys.*, 1985, **82**, 3045-3066.
11. M. H. Qiu, Z. F. Ren, L. Che, D. X. Dai, S. A. Harich, X. Y. Wang, X. M. Yang, C. X. Xu, D. Q. Xie, M. Gustafsson, R. T. Skodje, Z. G. Sun and D. H. Zhang, *Science*, 2006, **311**, 1440-1443.
12. L. Che, Z. Ren, X. Wang, W. Dong, D. Dai, X. Wang, D. H. Zhang, X. Yang, L. Sheng, G. Li, H.-J. Werner, F. Lique and M. H. Alexander, *Science*, 2007, **317**, 1061-1064.
13. W. Dong, C. Xiao, T. Wang, D. Dai, X. Yang and D. H. Zhang, *Science*, 2010, **327**, 1501-1502.
14. Z. F. Ren, Z. G. Sun, D. H. Zhang and X. M. Yang, *Rep. Prog. Phys.*, 2017, **80**, 02641.
15. M. Alagia, N. Balucani, L. Cartechini, P. Casavecchia, E. H. van Kleef, G. G. Volpi, F. J. Aoiz, L. Bañares, D. W. Schwenke, T. C. Allison, S. L. Mielke and D. G. Truhlar, *Science*, 1996, **273**, 1519-1522.
16. D. Skouteris, D. E. Manolopoulos, W. Bian, H.-J. Werner, L.-H. Lai and K. Liu, *Science*, 1999, **286**, 1713-1716.
17. X. Wang, W. Dong, C. Xiao, L. Che, Z. Ren, D. Dai, X. Wang, P. Casavecchia, X. Yang, B. Jiang, D. Xie, Z. Sun, S.-Y. Lee, D. H. Zhang, H.-J. Werner and M. H. Alexander, *Science*, 2008, **322**, 573-576.
18. T. G. Yang, J. Chen, L. Huang, T. Wang, C. L. Xiao, Z. G. Sun, D. X. Dai, X. M. Yang and D. H. Zhang, *Science*, 2015, **347**, 60-63.
19. S. A. Lahankar, J. Zhang, K. G. McKendrick and T. K. Minton, *Nat. Chem.*, 2013, **5**, 315–319.
20. S. A. Lahankar, J. Zhang, T. K. Minton and K. G. McKendrick, *J. Am. Chem. Soc.*, 2014, **136**, 12371-12384.
21. M. Alagia, N. Balucani, L. Cartechini, P. Casavecchia, E. H. v. Kleef, G. G. Volpi, P. J. Kuntz and J. J. Sloan, *J. Chem. Phys.*, 1998, **108**, 6698-6708.
22. Y.-T. Hsu, K. Liu, L. A. Pederson and G. C. Schatz, *J. Chem. Phys.*, 1999, **111**, 7921-7930.
23. X. Liu, J. J. Lin, S. Harich, G. C. Schatz and X. Yang, *Science*, 2000, **289**, 1536-1538.

24. M. Alagia, N. Balucani, L. Cartechini, P. Casavecchia, G. G. Volpi, L. A. Pederson, G. C. Schatz, G. Lendvay, L. B. Harding, T. Hollebeek, T.-S. Ho and H. Rabitz, *J. Chem. Phys.*, 1999, **110**, 8857-8860.
25. N. Balucani, L. Cartechini, G. Capozza, E. Segoloni, P. Casavecchia, G. G. Volpi, F. Javier Aoiz, L. Bañares, P. Honvault and J.-M. Launay, *Phys. Rev. Lett.*, 2002, **89**, 013201.
26. N. Balucani, G. Capozza, L. Cartechini, A. Bergeat, R. Bobbenkamp, P. Casavecchia, F. Javier Aoiz, L. Bañares, P. Honvault, B. Bussery-Honvault and J.-M. Launay, *Phys. Chem. Chem. Phys.*, 2004, **6**, 4957-4967.
27. N. Balucani, G. Capozza, E. Segoloni, A. Russo, R. Bobbenkamp, P. Casavecchia, T. Gonzalez-Lezana, E. J. Rackham, L. Bañares and F. J. Aoiz, *J. Chem. Phys.*, 2005, **122**, 234309.
28. Z. Shen, H. Ma, C. Zhang, M. Fu, Y. Wu, W. Bian and J. Cao, *Nat. Commun.*, 2017, **8**, 14094.
29. S.-H. Lee and K. Liu, *J. Phys. Chem. A*, 1998, **102**, 8637-8640.
30. S.-H. Lee and K. Liu, *Appl. Phys. B*, 2000, **71**, 627-633.
31. M. Lara, S. Chefdeville, K. M. Hickson, A. Bergeat, C. Naulin, J.-M. Launay and M. Costes, *Phys. Rev. Lett.*, 2012, **109**, 133201.
32. T. Wang, J. Chen, T. G. Yang, C. L. Xiao, Z. G. Sun, L. Huang, D. X. Dai, X. M. Yang and D. H. Zhang, *Science*, 2013, **342**, 1499-1502.
33. D. Yuan, Y. Guan, W. Chen, H. Zhao, S. Yu, C. Luo, Y. Tan, T. Xie, X. Wang, Z. Sun, D. H. Zhang and X. Yang, *Science*, 2018, **362**, 1289-1293.
34. M. Alagia, N. Balucani, P. Casavecchia, D. Stranges and G. G. Volpi, *J. Chem. Phys.*, 1993, **98**, 2459-2462.
35. B. R. Strazisar, C. Lin and H. Floyd Davis, *Science*, 2000, **290**, 958-961.
36. C. Xiao, X. Xu, S. Liu, T. Wang, W. Dong, T. Yang, Z. Sun, D. Dai, X. Xu, D. H. Zhang and X. Yang, *Science*, 2011, **333**, 440-442.
37. A. Sinha, M. C. Hsiao and F. F. Crim, *J. Chem. Phys.*, 1990, **92**, 6333-6335.
38. A. Sinha, M. C. Hsiao and F. F. Crim, *J. Chem. Phys.*, 1991, **94**, 4928-4935.
39. F. F. Crim, *Acc. Chem. Res.*, 1999, **32**, 877-884.
40. J. H. Wang, K. Liu, G. C. Schatz and M. ter Horst, *J. Chem. Phys.*, 1997, **107**, 7869-7875.
41. A. L. Brunsvold, J. Zhang, H. P. Upadhyaya, T. K. Minton, J. P. Camden, J. T. Paci and G. C. Schatz, *J. Phys. Chem. A*, 2007, **111**, 10907-10913.
42. A. Lagana, E. Garcia, A. Paladini, P. Casavecchia and N. Balucani, *Faraday Discuss.*, 2012, **157**, 415-436.
43. J. Li, J. Chen, D. H. Zhang and H. Guo, *J. Chem. Phys.*, 2014, **140**, 044327.
44. A. M. Zolot and D. J. Nesbitt, *J. Chem. Phys.*, 2008, **129**, 184305.
45. R. Otto, J. Y. Ma, A. W. Ray, J. S. Daluz, J. Li, H. Guo and R. E. Continetti, *Science*, 2014, **343**, 396-399.
46. J. Li, B. Jiang, H. Song, J. Ma, B. Zhao, R. Dawes and H. Guo, *J. Phys. Chem. A*, 2015, **119**, 4667-4687.
47. Z. Homayoon, J. M. Bowman, N. Balucani and P. Casavecchia, *J. Phys. Chem. Lett.*, 2014, **5**, 3508-3513.
48. W. Q. Zhang, Y. Zhou, G. R. Wu, Y. P. Lu, H. L. Pan, B. N. Fu, Q. A. Shuai, L. Liu, S. Liu, L. L. Zhang, B. Jiang, D. X. Dai, S. Y. Lee, Z. Xie, B. J. Braams, J. M. Bowman, M. A. Collins, D. H. Zhang and X. M. Yang, *Proc. Natl. Acad. Sci. U.S.A.*, 2010, **107**, 12782-12785.

49. J. J. Lin, J. Zhou, W. Shiu and K. Liu, *Science*, 2003, **300**, 966-969.
50. W. Shiu, J. J. Lin and K. P. Liu, *Phys. Rev. Lett.*, 2004, **92**, 103201.
51. W. Zhang, H. Kawamata and K. Liu, *Science*, 2009, **325**, 303-306.
52. F. Wang, J.-S. Lin and K. Liu, *Science*, 2011, **331**, 900-903.
53. F. Y. Wang, K. P. Liu and T. P. Rakitzis, *Nat. Chem.*, 2012, **4**, 636-641.
54. H. L. Pan, F. Y. Wang, G. Czako and K. P. Liu, *Nat. Chem.*, 2017, **9**, 1175-1180.
55. F. Wang and K. Liu, *Chem. Sci.*, 2010, **1**, 126-133.
56. B. Zhang, K. Liu and G. Czakó, *J. Phys. Chem. A*, 2015, **119**, 7190-7196.
57. B. Zhang, W. Shiu and K. Liu, *J. Phys. Chem. A*, 2005, **109**, 8983-8988.
58. B. Zhang, W. Shiu and K. Liu, *J. Phys. Chem. A*, 2005, **109**, 8989-8993.
59. J. J. Lin, J. Shu, Y. T. Lee and X. Yang, *J. Chem. Phys.*, 2000, **113**, 5287-5301.
60. H. Kohguchi, Y. Ogi and T. Suzuki, *Phys. Chem. Chem. Phys.*, 2011, **13**, 8371-8378.
61. Q. Shuai, H. Pan, J. Yang, D. Zhang, B. Jiang, D. Dai and X. Yang, *J. Chem. Phys.*, 2012, **137**, 224301.
62. N. Balucani, A. Bergeat, L. Cartechini, G. G. Volpi, P. Casavecchia, D. Skouteris and M. Rosi, *J. Phys. Chem. A*, 2009, **113**, 11138-11152.
63. F. Leonori, D. Skouteris, R. Petrucci, P. Casavecchia, M. Rosi and N. Balucani, *J. Chem. Phys.*, 2013, **138**, 024311.
64. C. Berteloite, S. D. Le Picard, I. R. Sims, M. Rosi, F. Leonori, R. Petrucci, N. Balucani, X. Wang and P. Casavecchia, *Phys. Chem. Chem. Phys.*, 2011, **13**, 8485-8501.
65. H. Pan, K. Liu, A. Caracciolo and P. Casavecchia, *Chem. Soc. Rev.*, 2017, **46**, 7517-7547.
66. A. M. Schmoltner, P. M. Chu, R. J. Brudzynski and Y. T. Lee, *J. Chem. Phys.*, 1989, **91**, 6926-6936.
67. R. I. Kaiser and A. M. Mebel, *Chem. Soc. Rev.*, 2012, **41**, 5490-5501.
68. D. S. N. Parker, A. M. Mebel and R. I. Kaiser, *Chem. Soc. Rev.*, 2014, **43**, 2701-2713.
69. R. I. Kaiser and N. Balucani, *Acc. Chem. Res.*, 2017, **50**, 1154-1162.
70. X. Gu, F. Zhang, Y. Guo and R. I. Kaiser, *Angew. Chem. Int. Ed.*, 2007, **46**, 6866-6869.
71. X. Gu, F. Zhang, Y. Guo and R. I. Kaiser, *J. Phys. Chem. A*, 2007, **111**, 11450-11459.
72. X. Gu and R. I. Kaiser, *Acc. Chem. Res.*, 2009, **42**, 290-302.
73. A. M. Mebel, V. V. Kislov and R. I. Kaiser, *J. Am. Chem. Soc.*, 2008, **130**, 13618-13629.
74. F. T. Zhang, S. Kim and R. I. Kaiser, *Phys. Chem. Chem. Phys.*, 2009, **11**, 4707-4714.
75. F. Zhang, S. Kim, R. I. Kaiser, A. Jamal and A. M. Mebel, *J. Chem. Phys.*, 2009, **130**, 234308.
76. S. B. Morales, C. J. Bennett, S. D. Le Picard, A. Canosa, I. R. Sims, B. J. Sun, P. H. Chen, A. H. H. Chang, V. V. Kislov, A. M. Mebel, X. Gu, F. Zhang, P. Maksyutenko and R. I. Kaiser, *Astrophys. J.*, 2011, **742**, 26.
77. D. S. N. Parker, A. V. Wilson, R. I. Kaiser, T. Labrador and A. M. Mebel, *J. Am. Chem. Soc.*, 2012, **134**, 13896-13901.
78. D. S. N. Parker, A. V. Wilson, R. I. Kaiser, T. Labrador and A. M. Mebel, *J. Org. Chem.*, 2012, **77**, 8574-8580.
79. D. S. N. Parker, F. Zhang, P. Maksyutenko, R. I. Kaiser and A. H. H. Chang, *Phys. Chem. Chem. Phys.*, 2011, **13**, 8560-8570.
80. D. S. N. Parker, F. Zhang, P. Maksyutenko, R. I. Kaiser, S. H. Chen and A. H. H. Chang, *Phys. Chem. Chem. Phys.*, 2012, **14**, 11099-11106.
81. S. J. Sibener, R. J. Buss, P. Casavecchia, T. Hirooka and Y. T. Lee, *J. Chem. Phys.*, 1980, **72**, 4341-4349.

82. R. J. Buss, R. J. Baseman, G. He and Y. T. Lee, *J. Photochem.*, 1981, **17**, 389-396.
83. A. M. Schmoltner, S. Y. Huang, R. J. Brudzynski, P. M. Chu and Y. T. Lee, *J. Chem. Phys.*, 1993, **99**, 1644-1653.
84. P. Casavecchia, G. Capozza, E. Segoloni, F. Leonori, N. Balucani and G. G. Volpi, *J. Phys. Chem. A*, 2005, **109**, 3527-3530.
85. F. Leonori, N. Balucani, G. Capozza, E. Segoloni, D. Stranges and P. Casavecchia, *Phys. Chem. Chem. Phys.*, 2007, **9**, 1307-1311.
86. F. Leonori, A. Occhiogrosso, N. Balucani, A. Bucci, R. Petrucci and P. Casavecchia, *J. Phys. Chem. Lett.*, 2012, **3**, 75-80.
87. F. Leonori, N. Balucani, G. Capozza, E. Segoloni, G. G. Volpi and P. Casavecchia, *Phys. Chem. Chem. Phys.*, 2014, **16**, 10008-10022.
88. C. Cavallotti, F. Leonori, N. Balucani, V. Nevrly, A. Bergeat, S. Falcinelli, G. Vanuzzo and P. Casavecchia, *J. Phys. Chem. Lett.*, 2014, **5**, 4213-4218.
89. P. Casavecchia, F. Leonori and N. Balucani, *Int. Rev. Phys. Chem.*, 2015, **34**, 161-204.
90. F. Leonori, N. Balucani, V. Nevrly, A. Bergeat, S. Falcinelli, G. Vanuzzo, P. Casavecchia and C. Cavallotti, *J. Phys. Chem. C*, 2015, **119**, 14632-14652.
91. G. Vanuzzo, N. Balucani, F. Leonori, D. Stranges, V. Nevrly, S. Falcinelli, A. Bergeat and P. Casavecchia, *J. Phys. Chem. A*, 2016, **120**, 4603-4618.
92. R. I. Kaiser, C. Ochsenfeld, M. Head-Gordon, Y. T. Lee and A. G. Suits, *Science*, 1996, **274**, 1508-1511.
93. R. I. Kaiser, C. Ochsenfeld, M. Head-Gordon, Y. T. Lee and A. G. Suits, *J. Chem. Phys.*, 1997, **106**, 1729-1741.
94. D. W. Chandler and P. L. Houston, *J. Chem. Phys.*, 1987, **87**, 1445-1447.
95. W. C. Wiley and I. H. McLaren, *Rev. Sci. Instrum.*, 1955, **26**, 1150-1157.
96. A. T. J. B. Eppink and D. H. Parker, *Rev. Sci. Instrum.*, 1997, **68**, 3477-3484.
97. M. Ahmed, D. S. Peterka and A. G. Suits, *Chem. Phys. Lett.*, 1999, **301**, 372-378.
98. P. A. Willis, H. U. Stauffer, R. Z. Hinrichs and H. F. Davis, *Rev. Sci. Instrum.*, 1999, **70**, 2606-2614.
99. P. A. Willis, H. U. Stauffer, R. Z. Hinrichs and H. F. Davis, *J. Phys. Chem. A*, 1999, **103**, 3706-3720.
100. H. U. Stauffer, R. Z. Hinrichs, P. A. Willis and H. F. Davis, *J. Chem. Phys.*, 1999, **111**, 4101-4112.
101. H. U. Stauffer, R. Z. Hinrichs, J. J. Schroden and H. F. Davis, *J. Chem. Phys.*, 1999, **111**, 10758-10761.
102. R. Z. Hinrichs, P. A. Willis, H. U. Stauffer, J. J. Schroden and H. F. Davis, *J. Chem. Phys.*, 2000, **112**, 4634-4643.
103. H. U. Stauffer, R. Z. Hinrichs, J. J. Schroden and H. F. Davis, *J. Phys. Chem. A*, 2000, **104**, 1107-1116.
104. J. J. Schroden, M. Teo and H. F. Davis, *J. Chem. Phys.*, 2002, **117**, 9258-9265.
105. J. J. Schroden, M. Teo and H. F. Davis, *J. Phys. Chem. A*, 2002, **106**, 11695-11699.
106. R. Z. Hinrichs, J. J. Schroden and H. F. Davis, *J. Am. Chem. Soc.*, 2003, **125**, 860-861.
107. R. Z. Hinrichs, J. J. Schroden and H. F. Davis, *J. Phys. Chem. A*, 2003, **107**, 9284-9294.
108. J. J. Schroden, C. C. Wang and H. F. Davis, *J. Phys. Chem. A*, 2003, **107**, 9295-9300.
109. R. Z. Hinrichs, J. J. Schroden and H. F. Davis, *J. Phys. Chem. A*, 2008, **112**, 3010-3019.
110. D. L. Proctor and H. F. Davis, *Proc. Natl. Acad. Sci. U.S.A.*, 2008, **105**, 12673-12677.
111. M. Ahmed, D. S. Peterka and A. G. Suits, *Phys. Chem. Chem. Phys.*, 2000, **2**, 861-868.

112. X. H. Liu, R. L. Gross, G. E. Hall, J. T. Muckerman and A. G. Suits, *J. Chem. Phys.*, 2002, **117**, 7947-7959.
113. R. L. Gross, X. H. Liu and A. G. Suits, *Chem. Phys. Lett.*, 2003, **376**, 710-716.
114. C. Huang, W. Li, A. D. Estillore and A. G. Suits, *J. Chem. Phys.*, 2008, **129**, 074301.
115. A. D. Estillore, L. M. Visger, R. I. Kaiser and A. G. Suits, *J. Phys. Chem. Lett.*, 2010, **1**, 2417-2421.
116. A. D. Estillore, L. M. Visger and A. G. Suits, *J. Chem. Phys.*, 2010, **132**, 164313.
117. A. D. Estillore, L. M. Visger and A. G. Suits, *J. Chem. Phys.*, 2010, **133**, 074306.
118. A. D. Estillore, L. M. Visger-Kiefer and A. G. Suits, *Faraday Discuss.*, 2012, **157**, 181-191.
119. B. Joalland, R. Van Camp, Y. Y. Shi, N. Patel and A. G. Suits, *J. Phys. Chem. A*, 2013, **117**, 7589-7594.
120. B. Joalland, Y. Shi, A. Kamasah, A. G. Suits and A. M. Mebel, *Nat. Commun.*, 2014, **5**, 4064.
121. B. Joalland, Y. Shi, N. Patel, R. Van Camp and A. G. Suits, *Phys. Chem. Chem. Phys.*, 2014, **16**, 414-420.
122. B. Joalland, Y. Y. Shi, A. D. Estillore, A. Kamasah, A. M. Mebel and A. G. Suits, *J. Phys. Chem. A*, 2014, **118**, 9281-9295.
123. Y. Shi, A. Kamasah and A. G. Suits, *J. Phys. Chem. A*, 2016, **120**, 8933-8940.
124. H. W. Li, A. Kamasah, S. Matsika and A. G. Suits, *Nat. Chem.*, 2019, **11**, 123-128.
125. H. W. Li, A. Kamasah and A. G. Suits, *Phys. Chem. Chem. Phys.*, 2019, **21**, 14186-14194.
126. D. Townsend, M. P. Minitti and A. G. Suits, *Rev. Sci. Instrum.*, 2003, **74**, 2530-2539.
127. C. R. Gebhardt, T. P. Rakitzis, P. C. Samartzis, V. Ladopoulos and T. N. Kitsopoulos, *Rev. Sci. Instrum.*, 2001, **72**, 3848-3853.
128. J. J. Lin, J. Zhou, W. Shiu and K. Liu, *Rev. Sci. Instrum.*, 2003, **74**, 2495-2500.
129. M. Ahmed, D. Blunt, D. Chen and A. G. Suits, *J. Chem. Phys.*, 1997, **106**, 7617-7624.
130. A. Kamasah, H. Li, J. Onvlee, A. van der Avoird, D. H. Parker and A. G. Suits, *Chem. Phys. Lett.*, 2018, **692**, 124-128.
131. C. Abeysekera, B. Joalland, Y. Shi, A. Kamasah, J. M. Oldham and A. G. Suits, *Rev. Sci. Instrum.*, 2014, **85**, 116107.
132. W. Li, S. D. Chambreau, S. A. Lahankar and A. G. Suits, *Rev. Sci. Instrum.*, 2005, **76**, 063106.
133. K. Kohse-Hoinghaus, P. Osswald, T. A. Cool, T. Kasper, N. Hansen, F. Qi, C. K. Westbrook and P. R. Westmoreland, *Angew. Chem. Int. Ed.*, 2010, **49**, 3572-3597.
134. A. C. Luntz and P. Andresen, *J. Chem. Phys.*, 1980, **72**, 5851-5856.
135. F. Ausfelder and K. G. McKendrick, *Prog. React. Kinet. Mec.*, 2000, **25**, 299-370.
136. D. Troya, *J. Phys. Chem. A*, 2019, **123**, 1044-1050.
137. D. Troya, *J. Phys. Chem. A*, 2019, **123**, 6911-6920.
138. G. T. Evans, E. van Kleef and S. Stolte, *J. Chem. Phys.*, 1990, **93**, 4874-4883.
139. E. S. Whitney, A. M. Zolot, A. B. McCoy, J. S. Francisco and D. J. Nesbitt, *J. Chem. Phys.*, 2005, **122**, 124310.
140. P. Andresen and A. C. Luntz, *J. Chem. Phys.*, 1980, **72**, 5842-5850.
141. J. P. Maillard, J. Chauville and A. W. Mantz, *J. Mol. Spectrosc.*, 1976, **63**, 120-141.
142. W. L. Meerts and A. Dymanus, *Chem. Phys. Lett.*, 1973, **23**, 45-47.

143. S. Rudić, C. Murray, D. Ascenzi, H. Anderson, J. N. Harvey and A. J. Orr-Ewing, *J. Chem. Phys.*, 2002, **117**, 5692-5706.
144. N. Balucani, *Chem. Soc. Rev.*, 2012, **41**, 5473-5483.
145. A. Lucassen, K. W. Zhang, J. Warkentin, K. Moshammer, P. Glarborg, P. Marshall and K. Kohse-Hoinghaus, *Combust. Flame*, 2012, **159**, 2254-2279.
146. M. A. El-Sayed, *J. Chem. Phys.*, 1963, **38**, 2834-2838.
147. M. A. El-Sayed, *Acc. Chem. Res.*, 1968, **1**, 8-16.
148. T. J. Preston, G. T. Dunning, A. J. Orr-Ewing and S. A. Vázquez, *J. Phys. Chem. A*, 2014, **118**, 5595-5607.
149. B. Hornung, T. J. Preston, S. Pandit, J. N. Harvey and A. J. Orr-Ewing, *J. Phys. Chem. A*, 2015, **119**, 9452-9464.
150. F. J. J. Cascarini, B. Hornung, M. S. Quinn, P. A. Robertson and A. J. Orr-Ewing, *J. Phys. Chem. A*, 2019, **123**, 2679-2686.
151. D. Townsend, S. A. Lahankar, S. K. Lee, S. D. Chambreau, A. G. Suits, X. Zhang, J. Rheinecker, L. B. Harding and J. M. Bowman, *Science*, 2004, **306**, 1158-1161.
152. A. G. Suits, *Acc. Chem. Res.*, 2008, **41**, 873-881.
153. L. B. Harding, S. J. Klippenstein and A. W. Jasper, *Phys. Chem. Chem. Phys.*, 2007, **9**, 4055-4070.
154. D. R. Albert, D. L. Proctor and H. F. Davis, *Rev. Sci. Instrum.*, 2013, **84**, 063104.
155. C. Amarasinghe and A. G. Suits, *J. Phys. Chem. Lett.*, 2017, **8**, 5153-5159.
156. C. Amarasinghe, H. Li, C. A. Perera, M. Besemer, A. van der Avoird, G. C. Groenenboom, C. Xie, H. Guo and A. G. Suits, *J. Phys. Chem. Lett.*, 2019, **10**, 2422-2427.
157. W. E. Perreault, N. Mukherjee and R. N. Zare, *Science*, 2017, **358**, 356-359.
158. W. E. Perreault, N. Mukherjee and R. N. Zare, *Nat. Chem.*, 2018, **10**, 561-567.
159. S. N. Vogels, J. Onvlee, S. Chefdeville, A. van der Avoird, G. C. Groenenboom and S. Y. T. van de Meerakker, *Science*, 2015, **350**, 787-790.
160. A. B. Henson, S. Gersten, Y. Shagam, J. Narevicius and E. Narevicius, *Science*, 2012, **338**, 234-238.
161. E. Lavert-Ofir, Y. Shagam, A. B. Henson, S. Gersten, J. Kłos, P. S. Żuchowski, J. Narevicius and E. Narevicius, *Nat. Chem.*, 2014, **6**, 332-335.
162. Y. Shagam, A. Klein, W. Skomorowski, R. Yun, V. Averbukh, C. P. Koch and E. Narevicius, *Nat. Chem.*, 2015, **7**, 921-926.
163. J. Jankunas, B. Bertsche, K. Jachymski, M. Hapka and A. Osterwalder, *J. Chem. Phys.*, 2014, **140**, 244302.
164. J. Jankunas, K. Jachymski, M. Hapka and A. Osterwalder, *J. Chem. Phys.*, 2015, **142**, 164305.
165. S. D. S. Gordon, J. J. Omiste, J. Zou, S. Tanteri, P. Brumer and A. Osterwalder, *Nat. Chem.*, 2018, **10**, 1190-1195.

Table of Contents Graphic

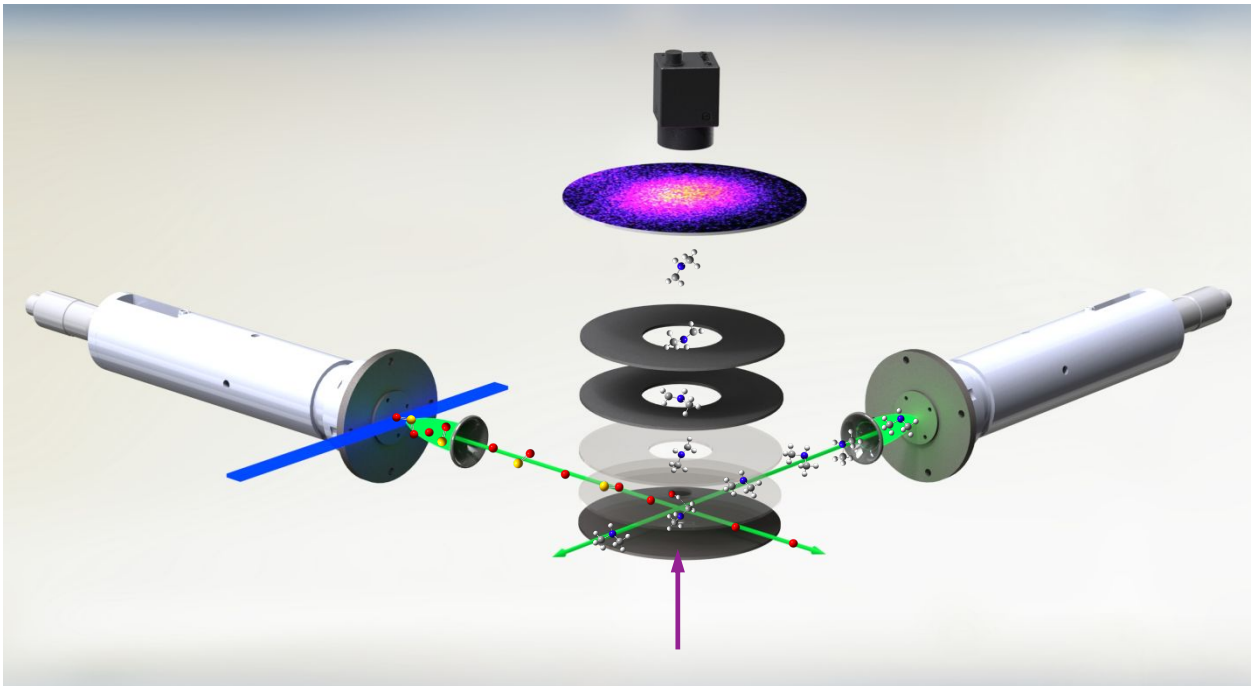

Crossed-beam imaging studies of polyatomic reactions show surprising dynamics not anticipated by extrapolation from smaller model systems.